JOURNAL OF GUIDANCE, CONTROL, AND DYNAMICS
Vol. 29, No. 5, September–October 2006

Spacecraft Formation Flight About Libration Points Using Impulsive Maneuvering

Henry J. Pernicka,* Brian A. Carlson,† and S. N. Balakrishnan‡
University of Missouri–Rolla, Rolla, Missouri 65409

DOI: 10.2514/1.18813

As more advanced spacecraft operational capabilities are required to accomplish innovative scientific missions, a shift to the incorporation of distributed space systems is under way. One area of current focus is the relative dynamics of a formation of spacecraft orbiting a libration point. One interesting and current challenge in this research area is maintaining formation control during both passive and active modes of operation, with different modes requiring different levels of accuracy. The research described in this paper focuses on the development and analysis of discrete maneuvering techniques using differential correction methods for maintaining a two satellite formation within required error tolerances for a given operational mode. In particular, formation sizes and control tolerances are sought for which impulsive maneuvering becomes a practical option.

Introduction

As more advanced spacecraft operational capabilities are required to accomplish innovative scientific missions, a shift from the use of traditional monolithic spacecraft toward systems of multiple spacecraft operating within a cooperative infrastructure is under way. Many new mission concepts have been proposed and will be proposed in the future that seek to utilize this decentralized approach termed distributed space systems (DSS). Research and development in this area aim toward making DSS a realistic option for incorporation into these mission designs.

A special case of this DSS concept involves formation flying of spacecraft where the continual maintenance of the relative separation and/or orientation is necessary. Much of the past research accomplished in the area of spacecraft formation flight has been applied to geocentric mission design [1–4]. However, in recent years significant attention has been devoted to the application of DSS technologies to libration point missions. Many of the features that make geocentric DSS architectures desirable are equally attractive near libration points, such as increased sensor resolution, lower cost, and simplified development of smaller individual satellites. Although the dynamics of a single spacecraft orbiting about a libration point are well known, one area of current focus is the relative dynamics of a formation of spacecraft at such a location. This study focuses on the use of impulsive maneuvers to maintain formation flight at a libration point, and in particular, formation sizes and control tolerances are sought for which impulsive maneuvering becomes a practical option.

To this end, the primary contribution of this study was to identify the allowable ranges of formation size and control "tolerance" for which ΔVs greater than a specified minimum "threshold" level could be used to maintain the formation. In other words, the types of formations that can be realistically maintained with discrete ΔVs were sought and identified. In this way, mission planners can quickly select mission architectures that are likely to be successful when impulsive thrusting is the desired control means onboard the spacecraft of the formation.

Previous Contributions

Recent years have seen an increase in Sun–Earth L_2 libration point mission studies due to the considerable interest in formation flight in this region. Orbits about the L_2 point are valued for their observational potential of distant objects from this region. With a spacecraft moving about the L_2 point the Sun, Earth, and Moon all appear in the same general direction, facilitating enhanced strategies for reducing the interference radiating from these bodies during data collection. This location also places the formation out of Earth's geomagnetic tail.

Formation flying has been defined as "the tracking or maintenance of a desired relative separation, orientation, or position between or among spacecraft."[§] Replacing traditional single large satellites with formations of multiple small satellites can be advantageous in many mission architectures. This decentralized approach in satellite mission design reduces the chance of catastrophic failure in one satellite, significantly impairing the function of the formation as a whole. This approach also "promotes agility, adaptability, evolvability, scalability, and affordability through the exploitation of multiple space platforms."[‖] A primary motivation in the development of formation flying techniques is the maintenance of a virtual aperture used for observing distant objects in space. "A virtual aperture is an effective aperture generated by a cluster of physically independent elements."[¶] These types of formations allow for higher resolution observations than with a single conventional aperture.

There are several technological challenges involved in implementing these types of formation missions. One is providing accurate and affordable relative tracking of individual satellites in the formation. Another is that in the mission design of virtual aperture formations, observational modes of operations have been defined that require the relative positions of each spacecraft in the formation to be controlled as tightly as 1 cm within their nominal separations [5,6]. Such a requirement creates the challenge of identifying hardware that can produce thrust controllable to very low magnitudes with sufficient accuracy to maintain the formation within this error tolerance.

Presented as Paper AAS-05-194 at the AAS/AIAA Space Flight Mechanics Meeting, Copper Mountain, Colorado, 23–27 January 2005; received 13 July 2005; revision received 18 January 2006; accepted for publication 19 January 2006.

*Associate Professor, Department of Mechanical and Aerospace Engineering; pernicka@umr.edu.

†Graduate Student, Department of Mechanical and Aerospace Engineering; bcarlson@umr.edu.

‡Professor, Department of Mechanical and Aerospace Engineering; bala@umr.edu.

§Glossary of Goddard Technology Management Office (GTMO) Terms," http://gsfctechnology.gsfc.nasa.gov [cited 10 June 2004].

‖"Distributed Space Systems," http://gsfctechnology.gsfc.nasa.gov [cited 28 July 2004].

¶"Distributed Space Systems," http://gsfctechnology.gsfc.nasa.gov [cited 28 July 2004].

Research in this area has focused on the development of control strategies involving both continuous and discrete thrusting techniques [7–11]. This study focuses on elements of formation control using impulsive thrusting techniques. Previous examinations of discrete techniques such as those in Marchand and Howell [12,13] examined the problem by dividing the trajectory into segments of a given time with impulsive maneuvers performed to maintain that path within a certain allowable error bound. Marchand and Howell [12,13] found that ΔV magnitudes in this region for small formation displacements and allowed error bounds can be prohibitively small for the given state of the art in propulsion technologies. However, in recent years, increasing interest in DSS and the required low-thrust levels have promoted advances in the development of propulsive devices that can produce very low thrust. One example of this promising technology is the development of colloid micro-Newton cold-gas thrusters with thrust levels in the 5–30 μN range [14]. For smaller spacecraft ($\sim$100 kg) planned for DSS missions such as the Stellar Imager, this results in an approximate attainable ΔV range of 1×10^{-6} to 1×10^{-5} m/s. Although all the necessary lifetime and performance testing have not been completed it appears that ΔV values in this range will be feasible in the near future.

Two goals of this effort, then, were to use numerical techniques to maximize the time spent within the error bounds before a maneuver is required and to achieve ΔV magnitudes that can be executed by currently available flight-tested propulsive hardware as well as propulsive hardware currently in development. The approach given here uses input parameters of formation displacement distance and allowable error bound and then fully exploits this error bound to maintain the formation using impulsive maneuvers of practical magnitude.

Basic Approach

Circular Restricted Three-Body Problem

An important initial step in this study was the identification of the dynamical model to be used. The circular restricted three-body problem (CR3BP) was chosen as the model in this research due to several reasons. One reason for its selection is in its ease of application to problems involving libration points. Another reason for selecting this model is its relative simplicity compared with other restricted or ephemeris-based "truth" models.

Figure 1 shows the geometry of the restricted three-body problem. Typically, the rotating reference frame is defined with origin at the libration point of interest or at the barycenter of the two-body system. In either case, the $\hat{\mathbf{x}}$ unit vector is typically directed from the larger primary toward the smaller primary. The $\hat{\mathbf{y}}$ unit vector is defined normal to the $\hat{\mathbf{x}}$ vector, within the plane of the primaries' orbit, and along the prograde rotational direction. The $\hat{\mathbf{z}}$ unit vector then completes the right-handed frame and is thus normal to the plane of the primaries' orbit. If the spacecraft is located by a position vector $\mathbf{r}$

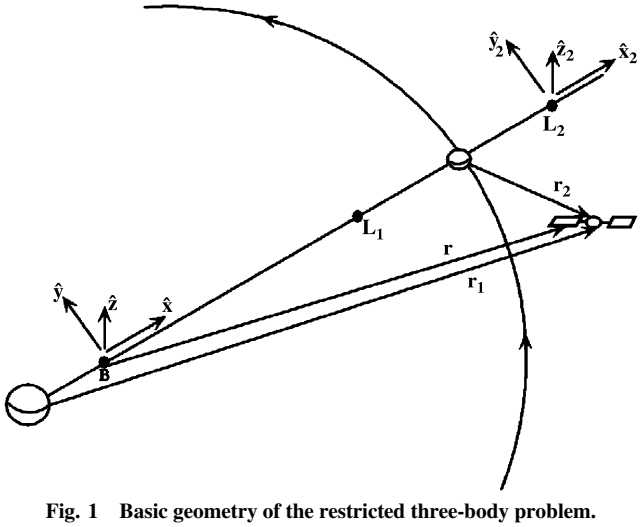

Fig. 1 Basic geometry of the restricted three-body problem.

with base point at the barycenter using coordinates x, y, and z with respect to the rotating frame, then the nondimensional equations of motion are given as

$$\begin{aligned}
\ddot{x} - 2\dot{\theta}\dot{y} - \dot{\theta}^2 x - \ddot{\theta} y &= -\frac{(1-\mu)(x+\mu R)}{r_1^3} - \frac{\mu[x-(1-\mu)R]}{r_2^3} \\
\ddot{y} + 2\dot{\theta}\dot{x} - \dot{\theta}^2 y - \ddot{\theta} x &= -\frac{(1-\mu)y}{r_1^3} - \frac{\mu y}{r_2^3} \\
\ddot{z} &= -\frac{(1-\mu)z}{r_1^3} - \frac{\mu z}{r_2^3}
\end{aligned} \tag{1}$$

assuming the primaries orbit the barycenter elliptically with their instantaneous separation given by R, and where μ is the ratio of the smaller primary's mass to the sum of both masses. In this study $R = 1$ is used to simplify the model to the circular restricted three-body problem (which then results in $\dot{\theta} = 1$ and $\ddot{\theta} = 0$).

Because there are no general closed-form solutions to the restricted three-body problem, approximate numeric and analytic solutions have been developed for computing halo or Lissajous orbits. The analytic approximations can be used to initiate numerical algorithms to compute precise trajectories using the dynamic model of interest. The method described by Howell and Pernicka [15] is used in this research to determine nominal Lissajous orbits.

Leader-Follower Concept

The primary consideration in this study was the identification of formation sizes and control tolerances that could be maintained by the use of impulsive maneuvers. In this study the "formation" is defined as a pair of spacecraft in a leader/follower configuration. However, the methods presented apply generally to a formation of almost any size and number of spacecraft.

Thus a simplified formation consisting of a leader spacecraft that orbits the L_2 libration point on a nominal Lissajous trajectory is defined, with amplitudes arbitrarily selected as $A_y = 300,000$ and $A_z = 200,000$ km. These dimensions were selected for study based on NASA's interest in research into formation flying about this type of trajectory. The nominal path was created using the method described in Howell and Pernicka [15] and was computed using the mass ratio $\mu = 3.040423 \times 10^{-6}$ corresponding to the Sun–Earth/Moon primary system. The other spacecraft in this formation is referred to as the follower spacecraft. The initial position of the follower spacecraft is defined by a desired displacement relative to the leader spacecraft, as shown in Eq. (2). The mission of interest typically determines the nominal relative displacement. Thus the initial position of the follower, relative to the barycenter and in terms of the rotating reference frame, is specified as

$$\begin{Bmatrix} x_o \\ y_o \\ z_o \end{Bmatrix}_{\text{follower}} = \begin{Bmatrix} x_o \\ y_o \\ z_o \end{Bmatrix}_{\text{leader}} + \begin{Bmatrix} \Delta x \\ \Delta y \\ \Delta z \end{Bmatrix}_{\text{desired}} \tag{2}$$

The initial velocity of the follower spacecraft is (temporarily) set equal to that of the leader spacecraft. The position and velocity of the leader on its nominal Lissajous trajectory and the initial relative position of the follower are then assumed to be fixed parameters. Therefore, adjusting the initial velocity of the follower spacecraft and implementing impulsive maneuvers when needed are the primary means used to accomplish the defined goals.

In the results presented, two different formation types were investigated. These formation types are designated the "*XYZ*" and "*xyz*" formations. For a given nominal formation displacement size ρ_o of the uppercase designation *XYZ* formation type is arbitrarily defined as

$$\begin{Bmatrix} \Delta x \\ \Delta y \\ \Delta z \end{Bmatrix}_{XYZ} = \begin{Bmatrix} \rho_o/\sqrt{3} \\ \rho_o/\sqrt{3} \\ \rho_o/\sqrt{3} \end{Bmatrix} \tag{3}$$

such that the follower is initially displaced and maintained equally along the inertial X, Y, and Z directions (which are omitted from Fig. 1 for clarity). In this case the formation geometry is fixed relative to inertial space. In contrast, the lowercase designation xyz formation is held fixed relative to the rotating frame and is equally displaced along the x, y, and z directions of the rotating frame in the same manner as shown in Eq. (3).

This leader–follower concept has some advantages and disadvantages compared with other formation concepts such as the virtual structure approach. In the leader–follower concept, as described previously, the motion of the follower is based on the motion of the leader. This condition implies the necessity of always knowing the states of the leader satellite. In the leader–follower model a failure in the leader is more easily imparted to the follower. One relatively new formation concept conceived to address this limitation is the virtual structure approach detailed in Ren and Beard [16]. This formation concept decentralizes the formation and works by having each spacecraft in a formation reference the motion of several nearby spacecraft in calculating control corrections instead of following one central leader spacecraft. This virtual structure approach may be better in actual mission control application in that it would result in more robust control methods because there is no single spacecraft from which the others of the formation are measured. However, the simplicity of the leader–follower concept and its "general" applicability to any two satellites in formation contributed to its selection in this research.

Trajectory Propagation

The algorithms developed for the purposes of propagating the equations of motion and implementing formation-keeping maneuvers were written using Matlab. In particular, the equations of motion were integrated using the ode113.m function with relative and absolute tolerances both set to 2.2×10^{-14}. Similarly, the check to determine whether the follower was within the error corridor was performed with a tolerance of 2.2×10^{-14} nondimensional units which results in a tolerance of slightly less than 1 cm. Finally Jacobi's Constant was numerically integrated simultaneously with the equations of motion and was found to vary less than approximately 1×10^{-15} (in nondimensional units) for a period of over 120 days, well beyond any overall segment duration propagated in this research.

Method Development

Numerous examples of control strategies applicable to formation flight are available in the literature. The focus in this work was the development of a relatively simple algorithm that allowed for maximum variation of parameters and variables in order to evaluate orders of magnitude of control input required to maintain a given formation. Most of the published control strategies are specifically designed to minimize both formation drift and ΔV. In this study, however, these two parameters were not specifically minimized. Instead, the time between formation-keeping maneuvers was the key metric to be maximized.

Thus the first attempts at maintaining the formation were accomplished using straightforward differential correction techniques. The goal was to increase the time spent in the error corridor (defined as a torus of specified radius $\delta_{\max}$ centered about the nominal path of the follower) to reduce the overall formation drift. The specific differential correction technique used is referred to as the "end-state targeting method." This method propagates the leader and follower states using CR3BP equations of motion, and uses the error in the relative displacement between the spacecraft at a given end time to correct the initial velocity of the follower to eliminate this error. In these first attempts the end time was defined (somewhat arbitrarily) as the time when the displacement of the follower violated the allowable displacement defined by the error corridor.

At the end time, the propagated follower spacecraft states are compared with the desired displacement as defined by the nominal position of the leader spacecraft that in turn defines the nominal position of the follower. This position error is then used in conjunction with the state transition matrix, ϕ, to iteratively generate corrections to the initial velocity of the follower spacecraft that results in the position at the end-time period corresponding to the desired (nominal) value. Because the desired position of the follower spacecraft is assumed to be defined by the mission requirements, as shown in Eq. (3), the state transition matrix relationship that relates changes in final states to changes in the final velocity can then be simplified to one that relates changes in the initial velocities to changes in the final positions as

$$\left[\left\{\begin{matrix}\dot{x}_o\\ \dot{y}_o\\ \dot{z}_o\end{matrix}\right\}_{\text{desired}} - \left\{\begin{matrix}\dot{x}_o\\ \dot{y}_o\\ \dot{z}_o\end{matrix}\right\}_{\text{actual}}\right] = \begin{bmatrix}\phi_{1,4} & \phi_{1,5} & \phi_{1,6}\\ \phi_{2,4} & \phi_{2,5} & \phi_{2,6}\\ \phi_{3,4} & \phi_{3,5} & \phi_{3,6}\end{bmatrix}^{-1}\left[\left\{\begin{matrix}x_f\\ y_f\\ z_f\end{matrix}\right\}_{\text{desired}} - \left\{\begin{matrix}x_f\\ y_f\\ z_f\end{matrix}\right\}_{\text{actual}}\right] \tag{4}$$

The desired position of the follower spacecraft is known throughout its entire trajectory, thus the propagated position at the end time can be compared with the desired position to determine the necessary ΔV to correct the path to the desired final position. Because the relationship in Eq. (4) is based on a linear approximation of the CR3BP about the L_2 libration point, several iterations of this process are required to converge to a small error tolerance (limited by the tolerance used with the integrator, 2.2×10^{-14} in nondimensional units or less than 1 cm).

Figure 2 shows a schematic diagram of the end-state targeting method over one trajectory segment [Fig. 2a] and its implementation over multiple segments [Fig. 2b]. In the figures, the nominal path of the leader satellite is shown with the nominal follower path at a specified displacement. The uncorrected propagated path is shown violating the error corridor (labeled in the figure as $\delta_{\max}$) and a maneuver is performed to correct the path so that it does not violate the corridor *and* intercepts the nominal path at the end of the segment. Recall that the end time for each segment in this method is defined as the time at which the corridor was violated during the original propagation during that given segment. The patching together of multiple segments as shown in Fig. 2b is referred to as "discrete ΔV end-state targeting," so-called due to the multiple applications of propulsive maneuvers required to maintain the follower location within the bounds of the error corridor.

In the discrete ΔV end-state targeting method shown in Fig. 2b the initial relative velocity of the follower was set to zero and as the trajectories are propagated the displacement between the two spacecraft will drift and eventually "violate" the corridor. The trajectory is analyzed to determine the exact time at which this violation occurs. This time interval from the initial time to the time of corridor violation is designated a "segment." Once the states of the leader and follower at this time have been determined, the end-state targeting method is employed to modify the initial velocity of the follower for the current segment so that the displacement error at the

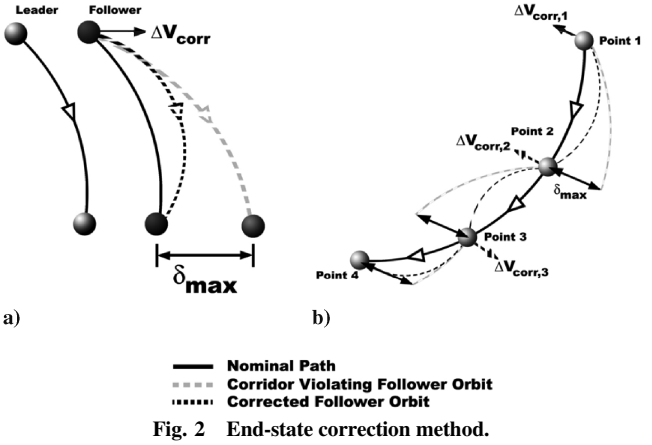

Fig. 2 End-state correction method.

Table 1 Formation-keeping summary: 10 m inertial formation/1.0 cm corridor

	ΔV (m/s)			
Time (days)	ΔV_x	ΔV_y	ΔV_z	$\Delta V_{\text{magnitude}}$
0.00	1.13E − 06	1.13E − 06	3.60E − 09	1.61E − 06
0.09	−6.42E − 08	4.59E − 08	5.70E − 08	9.74E − 08
1.35	−1.14E − 07	6.99E − 08	8.58E − 08	1.59E − 07
2.11	−9.39E − 08	5.82E − 08	7.23E − 08	1.32E − 07
3.05	−1.02E − 07	6.17E − 08	7.69E − 08	1.42E − 07

end time is reduced to zero. It should be noted that although the resulting trajectory between the start and end point is unlikely to exit (and reenter) the corridor, it possibly could. Checks are thus used to ensure this does not occur in the simulations developed for this study. However, in all simulations the follower trajectory was always significantly below the error corridor, and was found to be so far below that later iterations of this method sought to exploit this margin and to increase time in the corridor.

These modifications to the initial velocity at the beginning of a given segment are intended to represent discrete ΔVs that must be performed to maintain the follower satellite within the corridor. It should be noted that the correction at the beginning of the first segment is assumed to be an initial velocity achieved during the formation deployment, and thus is not considered to be a required formation-keeping maneuver. Table 1 lists the sample formation-keeping maneuvers calculated from using this method over five segments for an XYZ formation size of 10 m and an error corridor of 1 cm. Figure 3 shows the resulting variation in error vector magnitude as a function of time due to these maneuvers.

A review of the data in Table 1 shows that the ΔV magnitudes are all less than 1×10^{-7} m/s which is significantly lower than the approximately 0.1 m/s ΔVs generated by hardware used on past scientific missions such as the Solar and Heliospheric Observatory (SOHO) and Advanced Composition Explorer (ACE). However, these ΔVs are just 1 order of magnitude below the 1×10^{-6} to 1×10^{-5} m/s performance expected from micro-Newton cold-gas thruster technology. Regardless of the propulsive technology assumed available, it is evident that some method refinement is necessary to attain levels achievable by the developing cold-gas thruster technology.

Another consideration is the achievable accuracy of the executed ΔV even when a thruster is developed that can produce the needed magnitude. Preliminary results of testing the sensitivity of this method to error lead to a rule of thumb approximation that the error in the ΔV must be less than one-tenth of the magnitude. Thus for a desired 1×10^{-7} m/s correction, if the ΔV was in error by more than $\pm 1 \times 10^{-8}$ m/s the follower's trajectory segment following that maneuver would travel outside the error corridor. These results show that the technological challenges include not just achieving these small ΔVs but also achieving them quite accurately. To make more specific conclusions a Monte Carlo analysis outside the scope of this study is required.

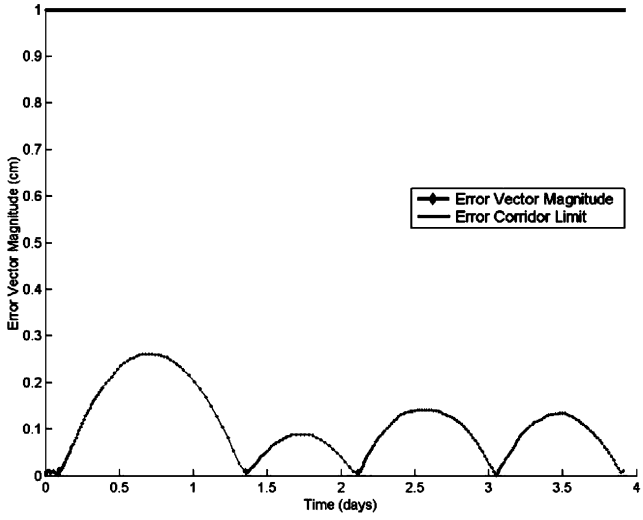

Fig. 3 Error magnitude for five segments (formation size = 10 m, error corridor size = 1 cm).

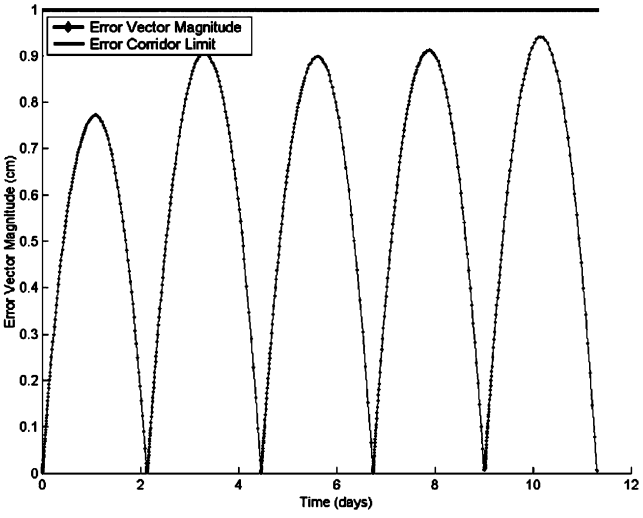

Fig. 4 Error magnitude for five segments using multiple corrections per segment (formation size = 10 m, error corridor size = 1 cm).

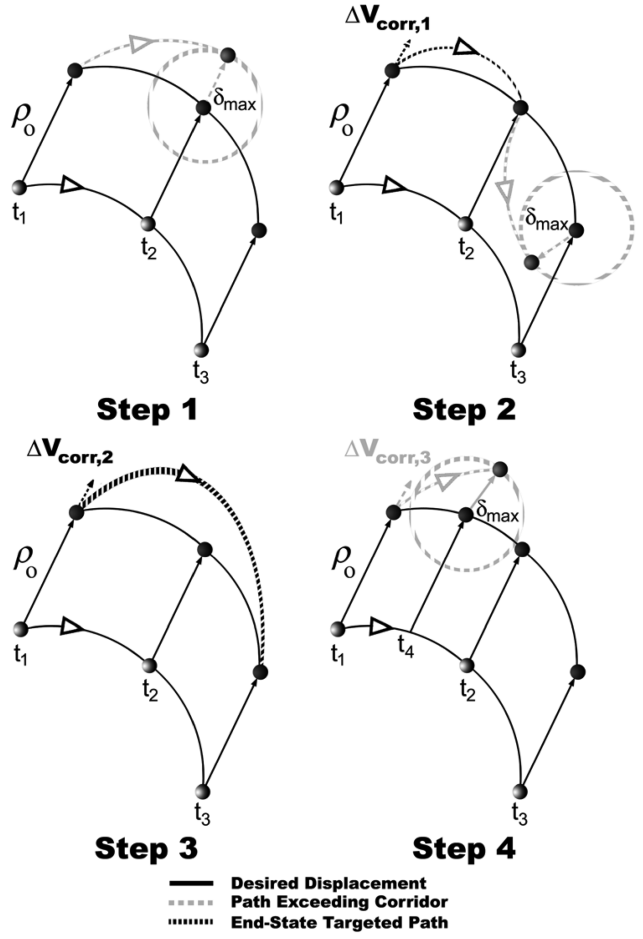

Fig. 5 Algorithm to increase time between maneuvers while remaining in the corridor.

Table 2 Comparison of parameters for single and multiple-correction methods for a 10 m *XYZ* formation with an error corridor size of 1.0 cm

	Total ΔV expended (m/s)	Average ΔV magnitude (m/s)	Total time in corridor (days)	Total ΔV cost (m/s per day)
Single correction	5.30E − 07	1.33E − 07	3.91	1.36E − 07
Multiple corrections	1.46E − 06	3.65E − 07	11.31	1.29E − 07

Table 3 Comparison of parameters for single and multiple-correction methods for a 600 km *XYZ* formation with an error corridor size of 30.0 km

	Total ΔV expended (m/s)	Average ΔV magnitude (m/s)	Total time in corridor (days)	Total ΔV cost (m/s per day)
Single correction	2.39E − 01	5.97E − 02	28.17	8.48E − 03
Multiple corrections	6.72E − 01	1.68E − 01	68.98	9.75E − 03

Table 4 Formation-keeping summary: 10 m inertial formation/1.0 cm error corridor

	ΔV (m/s)			
Time (days)	ΔV_x	ΔV_y	ΔV_z	$\Delta V_{\text{magnitude}}$
0.00	1.03E − 06	−1.08E − 06	9.05E − 08	1.49E − 06
2.14	−2.51E − 07	1.52E − 07	1.90E − 07	3.49E − 07
4.46	−2.65E − 07	1.56E − 07	1.97E − 07	3.66E − 07
6.74	−2.71E − 07	1.53E − 07	1.96E − 07	3.68E − 07
9.01	−2.84E − 07	1.53E − 07	1.97E − 07	3.78E − 07

Method Refinement

The next step in the modification of the algorithm to satisfy the defined goals was to attempt to maximize the time spent in the error corridor by manipulating the error magnitude behavior. This step was suggested by observing that the modified displacement trajectories (as shown in Fig. 3) did not "exploit" the entire available error corridor. To accomplish this modification, a second level of iterations was used to compute *each* segment, as opposed to the single level iteration used previously. End-state targeting was repeatedly performed on each segment until the time spent within the corridor was maximized. Figure 4 shows the result of maximizing the end time of each segment by modifying the initial velocities at the beginning of each segment using the same parameters used to produce Fig. 3.

Figure 5 demonstrates this stepwise process that increases the time spent in the error corridor. Step 1 shows how the natural trajectory of the follower given the original initial condition exceeds the error corridor $\delta_{\max}$ at time t_2. In step 2 of Fig. 5, a ΔV is performed that places the follower on a trajectory that remains within the corridor and now intersects the nominal path at time t_2, at which point the trajectory continues until it again exits the error corridor at time t_3. In step 3 a "refined" ΔV is computed and performed at t_1 to place the follower on a trajectory that remains within the error corridor until and beyond time t_3.

This process is repeated until the required ΔV refinement results in an end time t_4 shown that is less than t_3—thus that segment is discarded. The ΔV corresponding to the t_1-to-t_3 segment is then recorded as the ΔV that maximizes the time spent in the corridor for the first segment. Now the final states at the end of the first segment are used as the initial conditions for the second segment, and the process is repeated for the second segment.

Tables 2 and 3 compare the total ΔV expended, average ΔV, time in corridor, and ΔV cost per day of the single correction and multiple-correction methods for two different combinations of formations and error corridor sizes computed for five segments (thus requiring four maneuvers). The two formations were maintained in an orientation fixed relative to the inertial frame. It can be seen that this method results in an increase in the overall time in the corridor from 3.91 to 11.31 days for a 10-meter *XYZ* formation size and 1.0 cm error corridor. For a 600 km *XYZ* formation and 30 km error corridor the time increased from 28.17 to 68.98 days.

Table 5 Formation-keeping corridor variation summary: 10 m inertial formation

Error corridor size (cm)	Average ΔV magnitude (m/s)	Time in corridor (days)
1	3.61E − 07	11.17
2	5.16E − 07	15.67
3	6.32E − 07	18.95
4	7.35E − 07	21.80
5	8.25E − 07	24.19
6	9.00E − 07	26.20
7	9.75E − 07	28.19
8	1.05E − 06	29.94
9	1.11E − 06	31.69
10	1.17E − 06	33.22

Results

General Assumptions

Recall that a key goal used in compiling the results presented here is to maximize the time spent within the error corridor in each segment by fully exploiting the allowable error between the desired (nominal) and actual position states of the follower. This is in contrast to an approach that would attempt to drive the error as close to zero as possible along the entire trajectory, such as would typically be done when using continuous thrust. A related key assumption in this study is that the maximum error corridor specified corresponds to the allowable error at which the mission objectives are still fully achieved.

Results using the multiple-correction end-state methodology for maintaining the simple formation geometries used in this study have shown that is possible to increase the time spent in the corridor. Table 4 shows the results of performing this method with a 10-meter *XYZ* formation and an error corridor of 1.0 cm. Each row of this table represents the time at the beginning of a segment and the required impulsive maneuver components along $\hat{\mathbf{x}}$, $\hat{\mathbf{y}}$, and $\hat{\mathbf{z}}$ directions of the rotating frame with the corresponding ΔV magnitude. In all the results that are shown five segments were arbitrarily computed to allow for easy comparison of the effects of variation of the formation and error corridor sizes. It is expected that the method will work with any number of segments needed to satisfy mission duration requirements.

Table 5 shows the results of varying error corridor size from 1 to 10 cm for an XYZ formation size of 10 m. The ΔV magnitudes shown in Table 5 are the averages of the ΔVs performed over five segments of a given formation and error corridor set (such as the case shown in Table 4). The average ΔV magnitude was calculated by taking the average of all the impulsive maneuvers performed at the beginning of each segment except for the first maneuver. As previously mentioned, the first maneuver is assumed to be the necessary initial condition for the follower when the formation is initialized and thus is omitted from the average computation. The time in the corridor corresponds to the total time spent within the error corridor over all the segments.

Small Displacements and Error Corridors

As mentioned in the background, the overall goal of this study was to identify the allowable ranges of formation size and control tolerance for which ΔVs of a specified minimum threshold level could be used to maintain the formation. In reviewing Table 4 showing the performance of this method for an XYZ formation size of 10 m and an error corridor of 1.0 cm, the impulsive ΔVs necessary for maintaining the formation within the error corridor are on the order of 1×10^{-7} m/s in magnitude. Clearly this type of formation could not be maintained using impulsive maneuvers with currently available flight-certified hardware. However, for some of the larger error corridor size combinations shown in Table 5, the ΔV approaches the operating range of micro-Newton cold-gas thruster technology.

To quantify how formation size and error corridor bounds affect ΔV values and the total time spent within the error corridor, variation of parameter studies were conducted. Figure 6 shows the average ΔV magnitudes as a function of the error corridor sizes for XYZ formations with sizes ranging from 20 to 100 m. In this figure, each line represents the data for a single formation size and a set of error corridor sizes similar to the data shown in Table 5. From this figure it can be seen that for a given formation size, the average ΔV magnitude increases as the error corridor size is increased. Increasing the error corridor sizes allows the follower's relative velocity to increase as it takes advantage of having additional "room" to drift. These higher relative velocities then translate into higher ΔV magnitudes where each segment connects to the next one. An analogous trend is observed for increasing formation sizes for a given error corridor size. Figure 7 shows the total time in the error corridor as a function of error corridor sizes for XYZ formations with sizes ranging from 20 to 100 m corresponding to the parametric study shown in Fig. 6. The trend for each individual curve is similar to that in Fig. 6, in that for a given formation size it can be seen that overall time spent in the corridor increases as the error corridor size is increased. This increase is expected because the follower satellite can drift farther from its nominal trajectory before the corridor is violated. The overall trends in Fig. 7 vary from Fig. 6 in that the rate of increase of the time in corridor is larger for smaller formation sizes. In Fig. 6 the rate of increase of the average ΔV magnitudes grows for increasing formation sizes. The velocity difference between the leader and follower are again believed to be the root cause of these trends.

A smaller formation size will result in more time elapsing before the follower violates the error corridor. However, as mentioned before, any desired duration within the corridor can be achieved by simply computing additional segments until the needed time duration is reached during the final segment.

Although these results help to identify the trends generated from varying the formation and error corridor size they also make it apparent that at these particular formation dimensions the ΔVs required most likely cannot be performed using established propulsive technology and will most likely require micro-Newton cold-gas thrusters or similar low-thrust technology. Analyzing these formation/error corridor combinations demonstrate that the method can, at least mathematically, satisfy the goal of increasing the overall time spent in the corridor. When the formation sizes are increased into the 100 to 1000 km range as shown in Fig. 8, the average ΔV magnitudes, are easiliy with the range of developing propulsive hardware with magnitudes on the order of 1×10^{-4} m/s.

However, this magnitude of 1×10^{-4} m/s falls well short of a ΔV lower limit goal defined by esablished flight-tested propulsive hardware in this study as 0.1 m/s. This threshold was selected based on an examination of station keeping histories of the SOHO and ACE spacecraft. A review of [17,18] suggests the 0.1 m/s threshold as a reasonable choice for modeling established flight-tested hardware. As new advances in hardware reduce the threshold, smaller formation and error corridor sizes will become feasible and can be identified using the methods presented here.

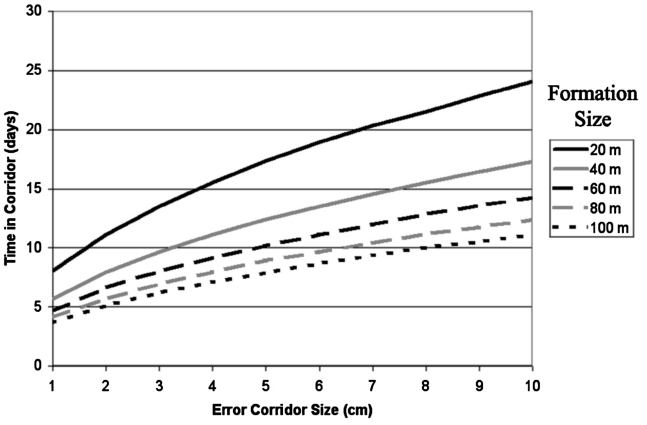

Fig. 7 Time in corridor as a function of error corridor size for varying XYZ formation sizes.

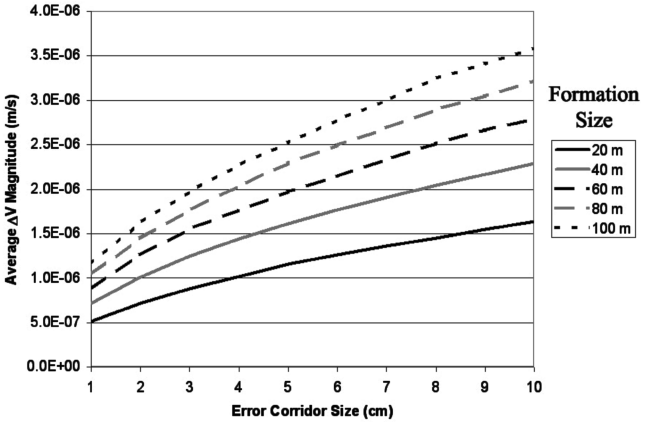

Fig. 6 Average magnitudes of impulsive maneuvers as a function of error corridor size for varying sizes of XYZ formations.

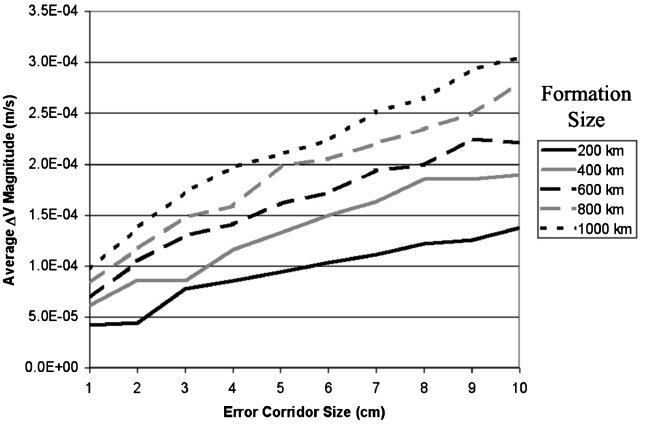

Fig. 8 Average magnitudes of impulsive maneuvers as a function of error corridor size for varying XYZ formations sizes.

Clearly, given a 0.1 m/s ΔV threshold and Figs. 6 and 8, it can be seen that impulsive control without the benefit of newer developing micro-Newton thrust technologies for the small corridor sizes that are currently required by proposed interferometry missions is impractical. However it may be of interest to future mission architectures to determine at what formation and corridor sizes impulsive control schemes become practical.

Practical Considerations

The selection of a maneuver threshold led to further variation of parameter studies to determine combinations of formation/error corridor sizes that do satisfy the 0.1 m/s threshold. Figure 9 shows average ΔV magnitudes as a function of error corridor sizes for XYZ formations ranging from 200 to 1000 km.

The figure shows that for a given desired formation size, there is a lower limit on reducing the error corridor size at which the ΔVs become impractical. However, as advancing micro-Newton thruster propulsive capabilities become available and flight tested, the ΔV threshold, allowable error corridor sizes, and formation sizes can be updated accordingly. Figure 10 shows an example of how a technological advance allowing the ΔV threshold to be reduced from 0.1 to an expected value of 1×10^{-5} for micro-Newton thrusters results in smaller possible formations and tighter formation control becoming possible. In actual application a mission planner can monitor further technological advances and determine what formation sizes are currently practical based on the ΔV threshold that is appropriate. Similarly, if the formation size was not negotiable, then the achievable error corridor size could be determined instead. For example, if a formation size of 200 m is required and the ΔVs are limited to greater than or equal to 1×10^{-5} m/s, then the achievable corridor size is limited to ~40 cm.

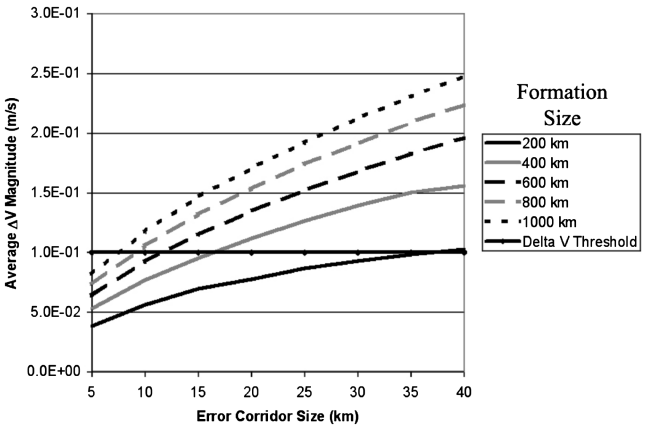

Fig. 9 Comparison of average ΔV to threshold ΔV for various error corridor sizes and formation sizes for XYZ formations.

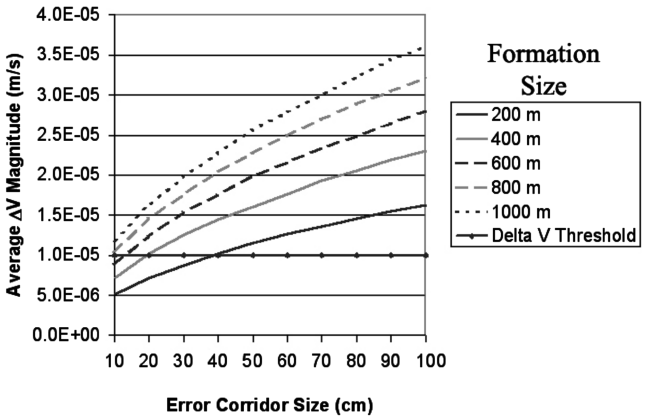

Fig. 10 Effect on error corridor size as threshold ΔV is decreased.

Rotational vs Inertial Formation Geometries

The results provided to this point all apply to inertially fixed XYZ formations. For missions that require inertial pointing, such as those observing phenomena in deep space, this is usually a necessity. However other missions may require fixed formations relative to the rotating frame of the Sun/Earth–Moon system. One example of a mission formation benefiting from being fixed relative to the rotating frame is a solar observation mission at the Sun–Earth L_1 location. Another example might be formation missions studying the Earth from orbit about the Sun–Earth L_2 point. Figure 11 shows the results from using the same analysis conducted to create Fig. 9 for formation orientations fixed relative to the rotational frame. A slight reduction in the rate of change of the average ΔV magnitudes in the rotational frame can be seen by comparing Figs. 9 and 11. Because both inertial and rotating formations require the follower to follow "nonnatural" paths, the maneuver trends can be difficult to identify. However, the rotational velocity with which both the leader and follower are initialized may explain the slightly lower maneuver histories for the rotational formation compared with the inertial formation.

Discussion of Method Sensitivity

In the previous results from this method it was found that for small formations ($\leq$ 100 m separation) and small error corridor sizes ($\leq$ 100 m) trends exist that relate the average ΔV magnitude and time spent in corridor as a function of the formation and error corridor size as shown in Figs. 6 and 7. These same trends emerged in Figs. 9 and 11 when practical displacement and error corridor size combinations were sought with formation sizes large ($200 \leq \rho_o \leq 1000$ km) and large error corridor sizes ($5 \leq \delta \leq 40$ km).

However, for small corridor sizes, if the formation is large these trends appeared to be less predictable. This difference can be seen by comparing Figs. 6 and 9 to Fig. 8. As such large formations are within the possible realm of operation of missions proposed for libration point regions, it was important to ensure that the reasons behind the lack of predictability were due to the dynamics of the system and not artifacts of the impulsive maneuvering method.

When the trend breakdown was first identified the initial thought was to assume that it was merely due to the chaotic nature of the L_2 region. In this region small changes in initial positions or velocities can result in large differences in future position and velocity. In the effort to confirm that this trend breakdown was caused by this chaotic nature and not by limitations in the method itself, the initial assumptions of the previous results were examined. One of the assumptions that immediately became suspect was the setting of the initial relative velocity of the follower spacecraft with respect to the leader equal to zero. This assumption was suspect due to the fact that the only difference between the results with consistent trends, Figs. 6 and 11, and the somewhat chaotic trends from the results in Fig. 8 was the approximate displacement to error corridor size ratios. In broad terms, both Figs. 6 and 11 resulted from relatively small displacement to error corridor size ratios resulting from the "small/small" and

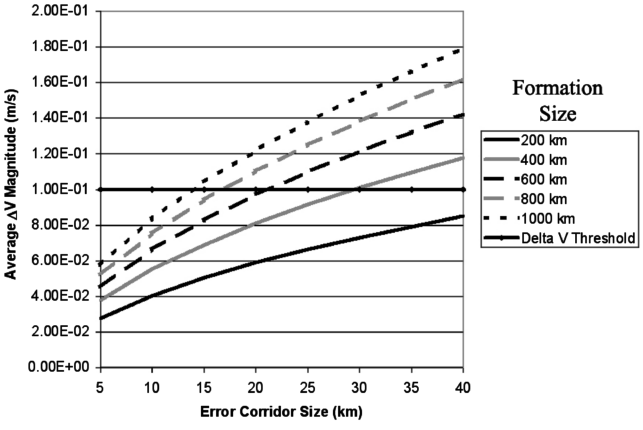

Fig. 11 Comparison of average ΔV to threshold ΔV for rotationally fixed xyz formations of varying corridor and formation sizes.

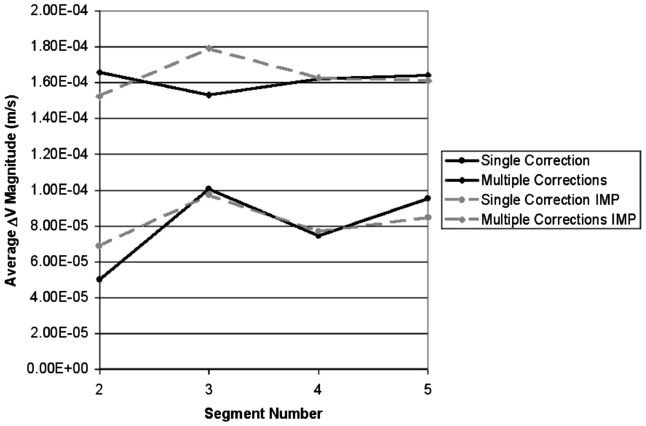

Fig. 12 Necessary ΔV correction magnitude for each segment (formation size = 600 km, error corridor size = 5 cm).

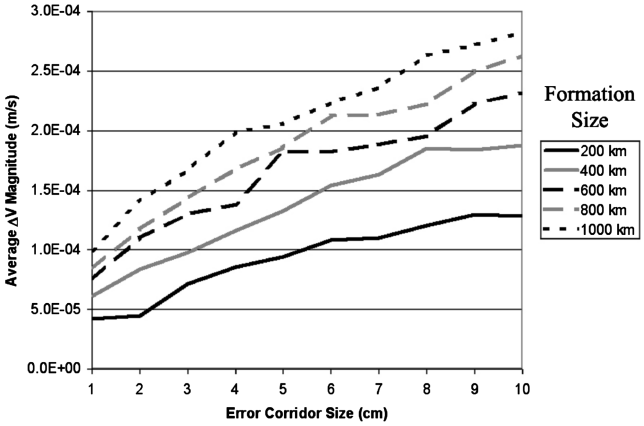

Fig. 13 Average magnitudes of impulsive maneuvers as a function of error corridor size for varying formation sizes using improved initial relative velocities.

"large/large" formation ratio combinations. The chaotic trend results in Fig. 8 however resulted from a "large/small" combination where relative displacement was much greater than the error corridor size.

In general as the displacement size between the two spacecraft increases the faster they drift more rapidly as their orbits are propagated. This is especially true when the initial relative velocity between the two spacecraft is set to zero. Without a proportionate increase in the error corridor size to keep the formation ratio from increasing a situation where the spacecraft exits a small corridor at a high rate of speed can develop resulting in very short exit times.

Referring to Fig. 5 that demonstrates how the end-state targeting technique is repeated to maximize the end time, it should be noted that the length of t_2 after the first iteration of the end-state targeting method is highly dependent on the original initial relative velocity. If a zero initial relative "seed" velocity (so-called because it initializes the method) causes t_2 to be much smaller than an improved initial relative velocity estimate might allow, then this small t_2 might create a ripple effect through the multiple iterations causing less predictable results. This ripple effect is evident in Fig. 12 which shows the ΔV corrections necessary at the beginning of each segment using combinations of single and multiple corrections and improved initial relative velocities.

When the technique described below is used to improve the initial relative velocities, the subsequent ΔV corrections significantly differ from those resulting from the original zero initial relative velocities. It should be noted that once again the initial ΔV correction is assumed to be absorbed into an overall initial formation nominal relative velocity and thus it is neglected in Fig. 12.

The approach taken was to determine the initial relative velocity between the leader and follower spacecraft that maximized the time spent in the allowable error corridor over the first trajectory segment. To accomplish this, the Matlab function "FMINSEARCH" was employed to minimize the reciprocal of the time duration recorded when the follower spacecraft error exited the allowable error corridor. From previous experience modifying the initial relative velocity for a single displacement and error corridor size combination it was determined that this solution, although not zero, would be near zero relative velocity and thus a zero relative velocity was used as the seed to initiate the search. Table 6 shows the difference in error corridor exit time for the original and improved initial relative velocities. It can be seen in this table that for various formation displacement and error corridor sizes that this method finds a relative velocity that better suits the formation compared with using the simple zero relative seed velocity approach. To recreate a plot similar to Fig. 8 it was necessary for this process to be repeated for each formation and error corridor size combination which resulted in a table of improved initial relative velocities to be used in conjunction with the multiple corrections method. The results of this combination can be seen in Fig. 13.

Table 6 Comparison of time spent in corridor over one segment for original and improved initial relative velocities

		Time spent in corridor (days)	
Formation displacement	Allowable error corridor	Original initial seed velocity	Improved initial seed velocity
20 m	1 cm	4.07E − 02	2.09E + 00
200 km	1 cm	6.39E − 06	4.35E − 05
200 km	20 km	1.09E + 01	2.87E + 01

Figure 13 shows the formation displacement and error corridor size combinations from Fig. 8 with the only difference being the use of the improved initial relative velocity. It is difficult to compare Figs. 8 and 13 and confidently conclude that displacement size lines have become less chaotic for the same displacement sizes or that the expected trends are followed more closely in Fig. 13 than in Fig. 8. For example, the traces for the 400 km formation size have become noticeably more evenly spaced and it can be seen that the predictability has been improved by using the improved initial relative velocity. However, the predictability of the 600 km formation size line has become degraded from Fig. 8 without the improved initial relative velocities.

Although the use of this improved initial relative velocity did not provide a completely consistent method extension for improving the predictability of these figures, these results help narrow down the possible causes of the lack of predictability. These results make it more plausible that the chaotic nature of the region is responsible for the trend breakdown and is not a complication with the method itself. Another possibility is that in these specific simulations the accuracy limits of the numerical integration are being reached. The chaotic results that were the subject of this analysis occurred when the ratio of formation size to error corridor was relatively large, such as a 1000 km formation with a 1 cm error corridor. This difference in scales used in the algorithm may be driving the unpredictability of the results.

Conclusions

General Conclusions

As expected and consistent with the extant literature regarding libration point formation-keeping, it was confirmed that small error corridor and formation sizes lead to ΔV magnitudes that are prohibitively small for established and flight-tested propulsion technology. However, new developments in the field of low-thrust micro-Newton propulsion have resulted in technologies that show promise for these challenging proposed scientific missions. The original method given here, derived from modification and experimentation with the differential correction technique, does successfully formation-keep in these regions as well as with large corridor sizes. The ΔV magnitudes range from 1×10^{-7} m/s for a 10-meter formation to 1×10^{-4} m/s for a 1000 km formation using a

1.0 cm error corridor. By parametrizing the ΔV magnitude as a function of the error corridor size for various formations sizes a range of error corridor and formation size combinations was determined that does result in average ΔV magnitudes at or above a ΔV threshold. This search of practical combinations resulted in more information than was previously available in the open literature regarding the identification of regimes at which impulsive maneuvers become practical. The resulting large error corridor sizes in the 5 to 40 km range using the 0.1 m/s threshold serve to further highlight the need for developing low-thrust micro-Newton cold-gas thrusters. As these new technologies are tested and verified in orbit, more precise ΔV thresholds can be defined for specific missions revealing the practical error corridor and formation size combinations for that technology.

A primary feature of the method presented in this paper is its somewhat nonstandard approach of exploiting the entire error corridor allowed by the mission of interest. In this way, the results of this study can be viewed as an approximate upper bound on required formation-keeping ΔV compared with optimized impulsive and even continuous control strategies. An approach that constantly drives the error between the two satellites to zero will likely require smaller ΔVs compared with the method presented here. However, in using the approach here a mission designer can be fairly certain on the order of magnitude level of the ΔVs required for a given formation and error corridor size combination.

Sensitivity of Method

In the Results section it was seen that the effect of these modifications resulted in improvement in consistency for some formation sizes but not others. Although this method did not establish fully consistent trend predictability, the process did allow the removal of one possible cause in the method. Although these sensitivity results do not fully ensure that the seemingly chaotic variation in the average ΔV magnitude is not an artifact of the impulsive maneuvering method, it removes the most likely candidate from the list of suspects. Another possible source of this inconsistency could be the inability of the numerical integration to produce sufficiently accurate results given the large difference in scales in the formation/error corridor size combinations where sensitivity was an issue.

Recommended Topics of Future Study

It should be noted that the results presented here were determined from within the framework of the CR3BP. Application of this method when using the elliptical restricted three-body problem (ER3BP) and ephemeris-based models including disturbances will increase the accuracy of this study and is a topic of future efforts. However, it is expected that the CR3BP provides a sufficiently accurate model to allow general conclusions to be made on the orders of magnitude of allowable formation and error corridor sizes when using impulsive maneuvers.

Another facet of this study that needs to be further explored is the use of varying formation geometries. As shown in Eq. (3) in the Basic Approach section, only one type of formation geometry was examined in this study. As such, this study does not provide an exhaustive and comprehensive examination of all possible combinations of formation geometry, size, and control tolerance. The trends shown in this study can be better generalized as different formation geometries and their respective sets of formation sizes and achievable accuracies are included in the results.

There is also need for refinement of the analysis of average ΔV as a function of error corridor size as more information on the performance of developing thruster technology becomes available. Also, other low-thrust options are also available to analyze, in addition to micro-Newton cold-gas thrusters. A goal of this study was to maintain a more general approach to the analysis throughout to provide a broad relevance to future mission design studies.

Finally it is important to also perform further verification that the unpredictability is due to the chaotic nature of the dynamics of the system. The fidelity levels that are achievable from dynamic models and their numerical integration are important subjects for future research in formation flight about libration points where extreme accuracy in position and pointing are usually required. Further verification is necessary to fully ensure that the unpredictability originates within the dynamics of the system and not from any as yet unrealized elements inherent to the method. However, the order of magnitude accuracy of the results presented here is still representative of the actual system.

Acknowledgments

This research was carried out at the University of Missouri–Rolla with support from the Graduate Student Research Program, NASA Goddard Space Flight Center, Grant Number NGT5-146.

References

[1] de Querirox, M.S., Kapila, V., and Yan, Q., "Adaptive Nonlinear Control of Multiple Spacecraft Formation Flying," *Journal of Guidance, Control, and Dynamics*, Vol. 23, No. 3, 2000, pp. 385–390.

[2] Inalhan G., Tillerson, M., and How, J. P., "Relative Dynamics and Control of Spacecraft Formations in Eccentric Orbits," *Journal of Guidance, Control, and Dynamics*, Vol. 25, No. 1, 2003, pp. 48–59.

[3] Sparks, A., "Linear Control of Spacecraft Formation Flying," AIAA Paper 2000-4438, 2000.

[4] Campbell, M. E., "Planning Algorithm for Multiple Satellite Clusters," *Journal of Guidance, Control, and Dynamics*, Vol. 26, No. 5, 2003, pp. 770–780.

[5] Carpenter, J. R., Leitner, J. A., Folta, D.C., and Burns, R. D., "Benchmark Problems for Spacecraft Formation Flying Missions," AIAA Paper 2003-5364, 2003.

[6] Bristow, J., Folta, D., and Hartman, K., "A Formation Flying Technology Vision," AIAA Paper 2000-5194, 2000.

[7] Vadali, S. R., Bae, H.-W., and Alfriend, K. T., "Design and Control of Libration Point Satellite Formations," AAS Paper 04-161, 2004.

[8] Scheeres, D. J., Hsiao, F.-Y., and Vinh, N. X., "Stabilizing Motion Relative to an Unstable Orbit: Applications to Spacecraft Formation Flight," *Journal of Guidance, Control, and Dynamics*, Vol. 26, No. 1, 2003, pp. 62–73.

[9] Wiesel, W. E., "Optimal Impulsive Control of Relative Satellite Motion," *Journal of Guidance, Control, and Dynamics*, Vol. 26, No. 1, 2003, pp. 74–78.

[10] Barden, B. T., Howell, K. C., and Lo, M. W., "Application of Dynamical Systems Theory to Trajectory Design for a Libration Point Mission," *AIAA/AAS Astrodynamics Conference, San Diego, CA*, Collection of Technical Papers (A96-34712 09-12), American Institute of Aeronautics and Astronautics, Reston, VA, 1996.

[11] Mitchell, J. W., and Richardson D. L., "Invariant Manifold Tracking for First-Order Nonlinear Hill's Equations," *Journal of Guidance, Control, and Dynamics*, Vol. 26, No. 4, 2003, pp. 622–627.

[12] Marchand, B. G., and Howell, K. C., "Formation Flight Near L_1 and L_2 in the Sun–Earth/Moon Ephemeris System Including Solar Radiation Pressure," AAS Paper 03-596, 2004.

[13] Marchand, B. G., and Howell, K. C., "Aspherical Formations Near the Libration Points in the Sun–Earth/Moon Ephemeris System," AAS Paper 04-157, 2004.

[14] Ziemer, J., Gamero-Castao, M., Hruby, V., Spence, D., Demmons, N., McCormick, R., Roy, T., Gasdaska, C., Young, J., and Connolly, B., "Colloid Micro-Newton Thruster Development for ST7-DRS and LISA Missions," AIAA Paper 2005-4265, 2005.

[15] Howell, K. C., and Pernicka, H. J., "Numerical Determination of Lissajous Trajectories in the Restricted Three-Body Problem," *Celestial Mechanics*, Vol. 41, Nos. 1–4, 1988, pp. 107–124.

[16] Ren, W., and Beard, R., "Decentralized Scheme for Spacecraft Formation Flying via the Virtual Structure Approach," *Journal of Guidance and Control*, Vol. 27, No. 1, 2004, pp. 73–82.

[17] Folta, D., and Hawkins, A., "Results of NASA's First Autonomous Formation Flying Experiment: Earth Observing-1 (EO-1)," AIAA Paper 2002-4743, 2002.

[18] Hamilton, N. H., and Folta, D., "Formation Flying Satellite Control Around L2 Sun–Earth Libration Point," AIAA Paper 2002-4528, 2002.